2018 IEEE/RSJ International Conference on Intelligent Robots and Systems (IROS), PREPRINT VERSION.
Madrid, Spain, October 1-5, 2018

Structure preserving Multi-Contact Balance Control for Series-Elastic and Visco-Elastic Humanoid Robots

Alexander Werner*, Bernd Henze*, Manuel Keppler*, Florian Loeffl*,
Sigrid Leyendecker†, Christian Ott*

***Abstract*— This paper proposes an integration of multi-body and actuator control for multi-contact balancing for robots with highly elastic joints. Inspired by the structure preserving control concept for series-elastic fixed-base robots, the presented approach aims to minimize the control effort by keeping the system structure intact. Balancing on multiple contacts requires to solve the force distribution problem. In locomotion, contacts change quickly, requiring a swift redistribution of contact forces. This is a challenge for elastic robots as the actuator dynamics and limits prevent instantaneous changes of contact forces. The proposed dynamically consistent force distribution is implemented as a model predictive controller which resolves redundancy while complying with contact force and actuator constraints.**

I. Introduction

Locomotion capabilities are essential for legged humanoid robots. For rigid robots, this problem has been in the focus of research for quite some time. However rigid humanoid robots still have little practical applications, partially because the risk of falling cannot fully be avoided by control, which creates the potential of mechanical damages. Elastic robots solve this robustness problem by smoothing impacts and enable efficiency gains for cyclic tasks such as locomotion. However, they also complicate the system dynamics by adding the state of the motor side. For series-elastic robots with high stiffness the effects can be dealt with on joint level by closed loop torque control. However, efficient locomotion requires lower stiffness values. This in turn necessitates treating the elasticity on multi-body level in the control approach.

For legged locomotion this means that the balancing and force distribution controllers have to consider the additional actuator dynamics. Conventional approaches for balancing assume full access to the contact forces or joint torques [1]–[3]. An example is our previously published passivity based multi-contact balancing controller [4] for rigid humanoid robots. This controller uses Cartesian impedance control of the center of mass (CoM) of the robot to create a stable balancing behavior. The advantage of using the passivity-based design is to minimize the reshaping of the system dynamics.

The same aspect is relevant for series-elastic robots, where we believe that passivity-based control approaches that preserve the system structure have a big potential. This was recently addressed by a structure preserving control for series-elastic systems (ESπ) [5] [6]. This control approach essentially implements a link-side torque interface on series-elastic robots.

Visco-elastic actuators [7] improve torque bandwidth and efficiency for creating link-side damping on elastic robots. Recently we transferred the structure preserving control concept to these joint types (VESπ) [8].

Previously we applied the multi-contact balancer with a motor-position based inner torque loop on our series-elastic legged robot C-Runner [9]. However the achieved performance especially for dynamic locomotion lags significantly behind the systems maximum capabilities, computed by optimal control [9]. One core problem was that the Cartesian tracking performance of link-side quantities was not adequate, because the approach did not account for the actuator dynamics and limits. We want to improve on this by applying a structure preserving control approach which models those limits explicitly.

Previous experiments showed that contact force dynamics generated by the balancing controller were not compatible with the actuator limits. This is resolved by the proposed dynamically consistent force distribution. Hereby the instantaneous force distribution problem for rigid robots is extended to a model predictive control problem. The latter respects the actuator dynamics and limits as well as contact force constraints.

With the increasing number of elastic legged robots, a number of control concepts were developed for such robots. Some approaches use operational-space control concepts to formulate the multi-body control part [10]–[12]. Inverse-dynamics approaches were also applied to successfully balance while walking [13]. In contrast to these related works, this paper does not focus on the multi-body part of the problem, instead the focus is on a closer integration of multi-body and series-elastic joint control. Integration of such approaches is also achieved with hybrid-zero dynamics based controllers [14], [15]. However, the solutions usually focus on the implementation of efficient cyclic locomotion. Also some of these robots exhibit very low mass legs which results in more

*The authors are with the Institute for Robotics and Mechatronics, German Aerospace Center (DLR). †The author is with the Department of Mechanical Engineering, University of Erlangen-Nuremberg.

This work was supported in part by the European Commission (H2020-ICT-645097 COMANOID).

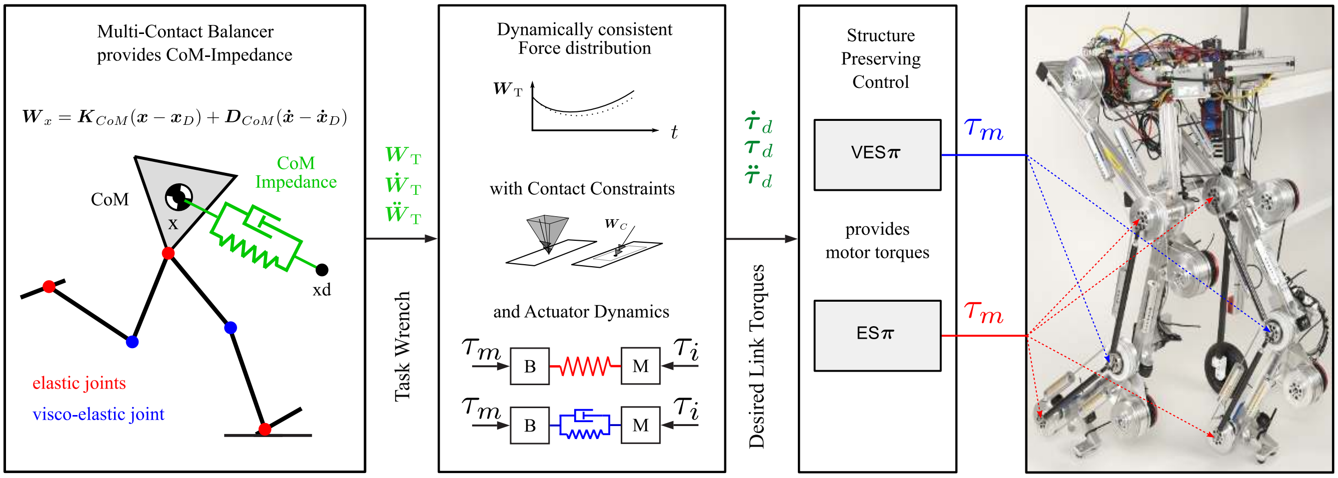

Fig. 1. Concept of the proposed balance controller for elastic systems. $\boldsymbol{W}_T$ are the task force and $\boldsymbol{\tau}_d$ are the desired link-side torques.

favorable relation between motor and link inertia. It must be stated that the problems addressed in this paper are most prevalent in robots which have significant link mass, and are designed for highly dynamic locomotion which results in significant motor inertia. We believe that future full-body humanoids designed for a large variety of applications, including significant locomotion performance, will have similar properties.

The presented approach targets our planar testbed robot, described in [16], which has a mixture of series-elastic and visco-elastic joints.

The remainder of the paper is organized as follows. First the assumed model is presented in section II. Section III summarizes the relevant parts of the multi-contact balancer. Section IV presents the core of the structure preserving control approaches for series-elastic and visco-elastic robots. Section V describes how both concepts can be combined. Section VI presents the novel dynamically consistent force distribution approach. Section VII describes the implementation and shows the simulation results. Section VIII concludes the paper.

II. Model

The minimal coordinates of the link-side are

$$\boldsymbol{y} = \begin{bmatrix} \boldsymbol{x} \\ \boldsymbol{q} \end{bmatrix} \in \mathbb{R}^{N_D} \tag{1}$$

with the under-actuated base coordinates $\boldsymbol{x} \in \mathbb{R}^{N_\mathrm{B}}$ and the joint coordinates $\boldsymbol{q} \in \mathbb{R}^{N_\mathrm{J}}$ actuated by elastic actuators. The link side dynamics of the robot is described by

$$\boldsymbol{M}(\boldsymbol{y})\ddot{\boldsymbol{y}} + \boldsymbol{C}(\boldsymbol{y},\dot{\boldsymbol{y}})\dot{\boldsymbol{y}} + \boldsymbol{g}(\boldsymbol{y}) = \begin{bmatrix} \boldsymbol{0} \\ \boldsymbol{\tau} \end{bmatrix} + \sum_{i=0}^{N_C} \boldsymbol{J}_{\mathrm{C,i}}^T(\boldsymbol{y})\boldsymbol{W}_{\mathrm{C,i}} \tag{2}$$

with the inertia matrix $\boldsymbol{M} \in \mathbb{R}^{N_D \times N_D}$, Coriolis matrix $\boldsymbol{C} \in \mathbb{R}^{N_D \times N_D}$, gravity terms $\boldsymbol{g} \in \mathbb{R}^{N_D}$, and joint torques $\boldsymbol{\tau} \in \mathbb{R}^{N_J}$. The robot has N_C contacts with the Jacobians $\boldsymbol{J}_{\mathrm{C,i}} \in \mathbb{R}^{6 \times N_D}$, and contact forces $\boldsymbol{W}_{\mathrm{C,i}} \in \mathbb{R}^6$. For clarity, the dependencies will be omitted for the remainder of the paper. The contact forces $\boldsymbol{W}_{\mathrm{C,i}}$ have to respect the inequality constraints formulating unilaterality, the friction cone, and the zero moment point (ZMP) to maintain a contact with the environment:

$$\boldsymbol{G}_{C,i}\boldsymbol{W}_{C,i} > \boldsymbol{0} \tag{3}$$

with the contact state dependant constraint matrix $\boldsymbol{G}_C$.

The motor dynamics are coupled to the link side dynamics only through linear springs forming an SEA or optionally with non-zero $\boldsymbol{D}$ a SVEA [17]:

$$\boldsymbol{B}\ddot{\boldsymbol{\theta}} = \boldsymbol{\tau}_m - \boldsymbol{\tau} \tag{4}$$

$$\boldsymbol{\tau} = \boldsymbol{K}(\boldsymbol{\theta} - \boldsymbol{q}) + \boldsymbol{D}(t)(\dot{\boldsymbol{\theta}} - \dot{\boldsymbol{q}}) \tag{5}$$

where $\boldsymbol{K} \in \mathbb{R}^{N_J \times N_J}$ is the stiffness matrix, $\boldsymbol{D} \in \mathbb{R}^{N_J \times N_J}$ the damping matrix, $\boldsymbol{\theta} \in \mathbb{R}^{N_J}$ the motor positions, $\boldsymbol{B} \in \mathbb{R}^{N_J \times N_J}$ the diagonal motor inertia matrix, and $\boldsymbol{\tau}_m \in \mathbb{R}^{N_J}$ the motor torque. The actuator dynamics is subject to constraints on the input $\boldsymbol{\tau}_\mathrm{m}$ and the velocity $\dot{\boldsymbol{\theta}}$:

$$-\dot{\boldsymbol{\theta}}_{\max} \leq \dot{\boldsymbol{\theta}} \leq \dot{\boldsymbol{\theta}}_{\max} \tag{6}$$

$$-\boldsymbol{\tau}_{\mathrm{m,max}} \leq \boldsymbol{\tau}_m \leq \boldsymbol{\tau}_{\mathrm{m,max}} \tag{7}$$

III. Multi-Contact Balancing for Rigid Humanoids

In order to maintain the balance, the controller stabilizes the CoM position $\boldsymbol{x}_\mathrm{c} \in \mathbb{R}^2$ and the hip orientation $\boldsymbol{R}_b \in \mathbb{R}^{2\times 2}$ by generating a Cartesian compliance force $\boldsymbol{W}_{\mathrm{x,d}} \in \mathbb{R}^3$ consisting of the stiffness matrix $\boldsymbol{K}_{\mathrm{CoM}}$ and damping matrix $\boldsymbol{D}_{\mathrm{CoM}}$. Each foot can be operated in two different modes. In *balancing mode*, the contacts are actively used for supporting the robot by generating the required contact wrenches $\boldsymbol{W}_{\mathrm{C,i}}$. In *interaction mode*, the pose of the foot is stabilized by a Cartesian compliance generating $\boldsymbol{W}_{C,i,d}$ which allows the foot to be lifted and moved to a different location. For a bipedal robot the vector of task wrenches is then defined as:

$$\boldsymbol{W}_T = \begin{bmatrix} \boldsymbol{W}_{x,d} \\ \boldsymbol{W}_{C,1,d} \\ \boldsymbol{W}_{C,2,d} \end{bmatrix} \tag{8}$$

As detailed in [4], the desired error dynamics of the closed loop system can be defined as

$$\boldsymbol{\Lambda}\begin{bmatrix}\Delta\dot{\boldsymbol{v}}_x\\ \Delta\dot{\boldsymbol{v}}_{\mathrm{C},1}\\ \Delta\dot{\boldsymbol{v}}_{\mathrm{C},2}\end{bmatrix}+\boldsymbol{\mu}\begin{bmatrix}\Delta\boldsymbol{v}_x\\ \Delta\boldsymbol{v}_{\mathrm{C},1}\\ \Delta\boldsymbol{v}_{\mathrm{C},2}\end{bmatrix}=\boldsymbol{W}_{\mathrm{ext}}-\begin{bmatrix}\boldsymbol{W}_{\mathrm{x,d}}\\ \boldsymbol{W}_{\mathrm{C,1,d}}\\ \boldsymbol{W}_{\mathrm{C,2,d}}\end{bmatrix} \tag{9}$$

with the end effector velocities $\boldsymbol{v}_{\mathrm{C,i}} = \boldsymbol{J}_{\mathrm{C,i}}\left[\,\boldsymbol{v}_{\mathrm{x}}^{\mathrm{T}}\ \dot{\boldsymbol{q}}^{\mathrm{T}}\,\right]^{\mathrm{T}}$. Note that the translational velocity of the CoM and the rotational velocity of the hip are stacked into $\boldsymbol{v}_{\mathrm{x}}$. The Cartesian inertia and Coriolis matrix are given by $\boldsymbol{\Lambda}$ and $\boldsymbol{\mu}$. The Δ in (9) denotes the difference between the actual state of the system and the desired trajectory. $\boldsymbol{W}_{\mathrm{ext}}$ combines all external wrenches acting on the end effectors.

Comparing (9) with the dynamic model in task space coordinates (detailed in [4]) leads to the controller, given here for the double support phase:

$$\begin{bmatrix}\boldsymbol{0}\\ \boldsymbol{\tau}_d\end{bmatrix}=\begin{bmatrix}m\boldsymbol{g}_0-\boldsymbol{W}_{\mathrm{x}}\\ \boldsymbol{0}\end{bmatrix}-\begin{bmatrix}\boldsymbol{J}_{\mathrm{C,1,u}}^{\mathrm{T}} & \boldsymbol{J}_{\mathrm{C,2,u}}^{\mathrm{T}}\\ \boldsymbol{J}_{\mathrm{C,1,l}}^{\mathrm{T}} & \boldsymbol{J}_{\mathrm{C,2,l}}^{\mathrm{T}}\end{bmatrix}\begin{bmatrix}\boldsymbol{W}_{\mathrm{C,1,d}}\\ \boldsymbol{W}_{\mathrm{C,2,d}}\end{bmatrix}+\begin{bmatrix}\boldsymbol{W}_{\mathrm{ff}}\\ \boldsymbol{\tau}_{\mathrm{ff}}\end{bmatrix} \tag{10}$$

with the total mass of the robot m, the gravity vector $\boldsymbol{g}_0$, the desired joint torques $\boldsymbol{\tau}_d$. The Jacobian matrices are partitioned into $\boldsymbol{J}_{\mathrm{C,i,u}}$ (non-actuated, related to $\boldsymbol{x}$), $\boldsymbol{J}_{\mathrm{C,i,l}}$ (actuated, related to $\boldsymbol{q}$). The last part $\boldsymbol{W}_{\mathrm{ff}}$ and $\boldsymbol{\tau}_{\mathrm{ff}}$ represents feed-forward terms similar to PD+ control as detailed in [4].

Note that the first line of (10) is underdetermined, which represents the force distribution problem of balancing on multiple end effectors. The redundancy is resolved and the task forces $\boldsymbol{W}_T$ are mapped to contact forces $\boldsymbol{W}_{C,i}$ by minimization of the cost function

$$\Gamma_T=\left\|\boldsymbol{G}\left[\begin{bmatrix}\boldsymbol{J}_{u,C,1}^T & \boldsymbol{J}_{u,C,1}^T\\ \boldsymbol{I} & \boldsymbol{0}\\ \boldsymbol{0} & \boldsymbol{I}\end{bmatrix}\begin{bmatrix}\hat{\boldsymbol{W}}_{C,1}\\ \hat{\boldsymbol{W}}_{C,2}\end{bmatrix}-\boldsymbol{W}_T\right]\right\| \tag{11}$$

with the positive semidefinite weight matrix $\boldsymbol{G}$. The values in $\boldsymbol{G}$ corresponding to the CoM task are constant. The value corresponding to the foot impedance forces are non-zero when the foot is not to be used in balancing mode. Additionally, the cost function is minimized with respect to the inequality constraints (3). This constraint quadratic optimization problem thus saturates the task wrenches $\boldsymbol{W}_T$ if they are not compatible with (3). The commanded joint torques $\boldsymbol{\tau}_d$ are computed from $\boldsymbol{W}_{C,i}$ via the lower part of (10).

IV. Structure preserving control of elastic robots

The next step is to realize the computed link-side torques $\boldsymbol{\tau}_d$ trough the serial-elastic and visco-elastic actuators. To this end, we apply ESπ and VESπ control that allow us to generate a torque series-elastic and visco-elastic robots while preserving the elastic structure and inertial properties. These control schemes are designed for the complete link-side and motor-side system. In this section only the torque-realizing part is described. The structure preserving impedance controller was previously used to control manipulators featuring a fixed-base [5].

A. Visco-Elastic Structure Preserving Impedance Control

Let us consider a fixed-base manipulator robot with visco-elastic actuators of the form (5). Defining the control input $\boldsymbol{\tau}_m$ as

$$\begin{aligned}\boldsymbol{\tau}_m =&\boldsymbol{B}\boldsymbol{D}^{-1}\Big(-\boldsymbol{D}\ddot{\boldsymbol{q}}+\Big(\dot{\boldsymbol{D}}+\boldsymbol{\kappa}(\boldsymbol{\eta}-\boldsymbol{q})\Big)(\dot{\boldsymbol{\eta}}-\dot{\boldsymbol{q}})\Big)\\ &+\boldsymbol{B}\boldsymbol{D}^{-1}(\dot{\hat{\boldsymbol{\tau}}}-\dot{\boldsymbol{D}}\dot{\boldsymbol{\theta}})+\boldsymbol{\tau}_d-\boldsymbol{D}_\eta\dot{\boldsymbol{\eta}},\end{aligned} \tag{12}$$

where

$$\hat{\boldsymbol{\tau}} =\boldsymbol{D}\dot{\boldsymbol{q}}-\boldsymbol{K}(\boldsymbol{\theta}-\boldsymbol{q})+\boldsymbol{\tau}_d. \tag{13}$$

This yields the following link and motor dynamics

$$\boldsymbol{M}_{\boldsymbol{q}}(\boldsymbol{q})\ddot{\boldsymbol{q}}+\boldsymbol{C}_{\boldsymbol{q}}(\dot{\boldsymbol{q}},\boldsymbol{q})+\boldsymbol{g}_{\boldsymbol{q}}(\boldsymbol{q}) =\boldsymbol{\tau}_v(\dot{\boldsymbol{\eta}},\boldsymbol{\eta},\dot{\boldsymbol{q}},\boldsymbol{q})+\boldsymbol{\tau}_d \tag{14}$$

$$\boldsymbol{B}\ddot{\boldsymbol{\eta}}+\boldsymbol{\tau}_v(\dot{\boldsymbol{\eta}},\boldsymbol{\eta},\dot{\boldsymbol{q}},\boldsymbol{q}) =-\boldsymbol{D}_\eta\dot{\boldsymbol{\eta}}. \tag{15}$$

where $\boldsymbol{M}_{\boldsymbol{q}}$, $\boldsymbol{C}_{\boldsymbol{q}}$, and $\boldsymbol{g}_{\boldsymbol{q}}$ describe the dynamic properties of the manipulator robot. The new motor coordinates $\boldsymbol{\eta}$ are implicitly defined via the following coordinate transformation

$$\boldsymbol{\tau}_v(\dot{\boldsymbol{\theta}},\boldsymbol{\theta},\dot{\boldsymbol{q}},\boldsymbol{q})=\boldsymbol{\tau}_v(\dot{\boldsymbol{\eta}},\boldsymbol{\eta},\dot{\boldsymbol{q}},\boldsymbol{q})+\boldsymbol{\tau}_d(t,\dot{\boldsymbol{q}},\boldsymbol{q}). \tag{16}$$

B. Elastic Structure Preserving Impedance Control

For an equivalent manipulator with series-elastic actuators of the form (5) with $\boldsymbol{D}=0$ defining the control input as

$$\boldsymbol{\tau}_m=\boldsymbol{B}\boldsymbol{K}^{-1}\ddot{\boldsymbol{\tau}}_d+\boldsymbol{\tau}_d-\boldsymbol{D}_\eta\dot{\boldsymbol{\eta}} \tag{17}$$

yields the following link and motor dynamics

$$\boldsymbol{M}_{\boldsymbol{q}}(\boldsymbol{q})\ddot{\boldsymbol{q}}+\boldsymbol{C}_{\boldsymbol{q}}(\dot{\boldsymbol{q}},\boldsymbol{q})+\boldsymbol{g}_{\boldsymbol{q}}(\boldsymbol{q}) =\boldsymbol{\tau}_e(\dot{\boldsymbol{\eta}},\boldsymbol{\eta},\dot{\boldsymbol{q}},\boldsymbol{q})+\boldsymbol{\tau}_d \tag{18}$$

$$\boldsymbol{B}\ddot{\boldsymbol{\eta}}+\boldsymbol{\tau}_e(\dot{\boldsymbol{\eta}},\boldsymbol{\eta},\dot{\boldsymbol{q}},\boldsymbol{q}) =-\boldsymbol{D}_\eta\dot{\boldsymbol{\eta}}. \tag{19}$$

The new motor coordinates $\boldsymbol{\eta}$ are implicitly defined via the following coordinate transformation

$$\boldsymbol{\tau}_e(\dot{\boldsymbol{\theta}},\boldsymbol{\theta},\dot{\boldsymbol{q}},\boldsymbol{q})=\boldsymbol{\tau}_e(\dot{\boldsymbol{\eta}},\boldsymbol{\eta},\dot{\boldsymbol{q}},\boldsymbol{q})+\boldsymbol{\tau}_d(t,\dot{\boldsymbol{q}},\boldsymbol{q}). \tag{20}$$

An appropriate design of motor damping matrix $\boldsymbol{D}_\eta$ is given in [5]

This controller realizes $\boldsymbol{\tau}_d$ with the exception of the disturbance caused by the motor inertia $\boldsymbol{B}$ (which can still be shaped). Note that derivatives of the desired torque up to $\ddot{\boldsymbol{\tau}}_{\boldsymbol{d}}$ have to be provided.

V. Elastic Balancing

The balancing scheme described in section III uses task wrenches $\boldsymbol{W}_T$ to stabilize the robot which are distributed onto the available contacts. These contact forces $\boldsymbol{W}_{C,i,d}$ are then realized via $\boldsymbol{J}_{C,i,l}^T$ and the desired torques $\boldsymbol{\tau}_d$, which represent the control input on non-elastic humanoid robots.

For elastic robots $\boldsymbol{\tau}_i$, the link torques $\boldsymbol{\tau}$ can only be accessed indirectly via the actuator dynamics. The structure preserving control approach presented in section IV provides a method to apply a balancing controller which assumes rigid joints (as the one described in section III) to a robot with elastic joints while preserving the structure of the system dynamics.

Combining the balancing controller (Section III) with the ESP/VESP concept (Section IV) results in the control architecture which is illustrated in Fig. I: the link side impedance part, which consists of the multi-contact balancer plus the dynamically consistent force distribution, and the motor side part, which is represented by the ESP/VESP controller. The resulting closed loop dynamics of combination of the balancing and the ESP/VESP controller is derived in the appendix.

No formal stability analysis of the complete structure is presented in this paper. It is just pointed out that both, multi-contact balancing and $ES\pi/VESP\pi$, have individual stability proofs. For the multi-contact balancer there is the restriction that the task wrenches $\boldsymbol{W}_T$ need to be realizable with the available contacts, that the contacts with the environment actually exist, and that the configuration is not singular [4].

VI. Dynamically consistent force distribution

Note that the instantaneous force distribution of the balancer presented in section III does not account for the actuator dynamics and limitations, which can lead to a mismatch between the desired and the realized wrenches, especially in transient situations. On non-elastic humanoid robots, an instantaneous redistribution of the load between contacts is possible when no underlying dynamics is assumed. For elastic humanoids an instantaneous redistribution would require a step in $\boldsymbol{\tau}_d$, which is physically not possible due to the actuator dynamics. Note that this problem can be triggered when the contact force constraints (3) switch from a deactivated into an activated state. In this case $\dot{\boldsymbol{\tau}}_d$ is not continuous anymore and thus cannot be tracked by the actuators. These problems of an instantaneous force distribution are now remedied by the use of a model predictive control approach which resolves the force distribution problem, respects the actuator dynamics (4), and actuator constraints (7) (see next section).

The dynamically consistent force distribution improves the instantaneous force distribution described in section III. It is a way to integrate the following aspects into one controller:

- Minimizing the deviation between the desired task wrenches $\boldsymbol{W}_T$ and the realized ones
- Contact wrench constraints (3)
- Contact wrench redundancy resolution (10)
- *Actuator constraints on $\boldsymbol{\tau_m}$ and $\dot{\boldsymbol{\theta}}$* (7)
- *Regularization on control input $\boldsymbol{\tau}_m$ instead of the contact wrenches as in [9]*

where the last two items are novel contributions. Note that constraints require a preview of the actuator dynamics and therefore lead to a model predictive controller.

The basic mapping of the task wrenches $\boldsymbol{W}_T$ stays the same as in the instantaneous force distribution approach. The contact wrenches $\boldsymbol{W}_{C,i}$ can be by associated motor positions $\hat{\boldsymbol{\theta}}$ and motor velocities $\dot{\hat{\boldsymbol{\theta}}}$ in a singularity free configuration by:

$$\begin{bmatrix}\hat{\boldsymbol{W}}_{C,1}\\ \hat{\boldsymbol{W}}_{C,2}\end{bmatrix} = \begin{bmatrix}\boldsymbol{J}_{C,1,l}^{-T}\\ \boldsymbol{J}_{C,2,l}^{-T}\end{bmatrix}\hat{\boldsymbol{\tau}}_d = \begin{bmatrix}\boldsymbol{J}_{C,1,l}^{-T}\\ \boldsymbol{J}_{C,2,l}^{-T}\end{bmatrix}\begin{bmatrix}\boldsymbol{K} & \boldsymbol{D}\end{bmatrix}\left[\begin{bmatrix}\hat{\boldsymbol{\theta}}\\ \dot{\hat{\boldsymbol{\theta}}}\end{bmatrix} - \begin{bmatrix}\boldsymbol{q}\\ \dot{\boldsymbol{q}}\end{bmatrix}\right] \tag{21}$$

Note that $\hat{\boldsymbol{\theta}}$ and $\dot{\hat{\boldsymbol{\theta}}}$ are just internal variables of the force distribution algorithm and are not passed to the $\mathrm{ES}\pi/\mathrm{VES}\pi$ control as Fig. I illustrates. The mapping of the contact force to task forces and (21) can be combined into:

$$\begin{aligned}\boldsymbol{W}_T = \quad & \boldsymbol{P}\left[\begin{bmatrix}\hat{\boldsymbol{\theta}}\\ \dot{\hat{\boldsymbol{\theta}}}\end{bmatrix} - \begin{bmatrix}\boldsymbol{q}\\ \dot{\boldsymbol{q}}\end{bmatrix}\right]\\ \boldsymbol{P} = & \begin{bmatrix}\boldsymbol{J}_{C,1,u}^T & \boldsymbol{J}_{C,2,u}^T\\ \boldsymbol{I} & \boldsymbol{0}\\ \boldsymbol{0} & \boldsymbol{I}\end{bmatrix}\begin{bmatrix}\boldsymbol{J}_{C,1,l}^{-T}\\ \boldsymbol{J}_{C,2,l}^{-T}\end{bmatrix}\begin{bmatrix}\boldsymbol{K} & \boldsymbol{D}\end{bmatrix}\end{aligned} \tag{22}$$

which comprises the link side configuration dependant aspect ($\boldsymbol{J}_{C,i}$) of the system dynamics. Note that the force distribution only works on the motor side dynamics and assumes that the state of the link side is known. This can be justified by the different time constants of the link side and the motor side.

The linear actuator dynamics can be written in state space form as:

$$\begin{aligned}\underbrace{\frac{\partial}{\partial t}\begin{bmatrix}\boldsymbol{\theta}\\ \dot{\boldsymbol{\theta}}\end{bmatrix}}_{\dot{\boldsymbol{\Theta}}} = & \underbrace{\begin{bmatrix}\boldsymbol{0} & \boldsymbol{I}\\ -\boldsymbol{B}^{-1}\boldsymbol{K} & -\boldsymbol{B}^{-1}\boldsymbol{D}\end{bmatrix}}_{\boldsymbol{A}^*}\underbrace{\begin{bmatrix}\boldsymbol{\theta}\\ \dot{\boldsymbol{\theta}}\end{bmatrix}}_{\boldsymbol{\Theta}} + \underbrace{\begin{bmatrix}\boldsymbol{0}\\ \boldsymbol{B}^{-1}\end{bmatrix}}_{\boldsymbol{B}^*}\boldsymbol{\tau}_{\mathrm{m}} +\\ & + \underbrace{\begin{bmatrix}\boldsymbol{0} & \boldsymbol{0}\\ \boldsymbol{B}^{-1}\boldsymbol{K} & \boldsymbol{B}^{-1}\boldsymbol{D}\end{bmatrix}}_{\boldsymbol{G}^*}\begin{bmatrix}\boldsymbol{q}\\ \dot{\boldsymbol{q}}\end{bmatrix}\end{aligned} \tag{23}$$

which is a linear system with known disturbance in form of $\boldsymbol{q}$ and $\dot{\boldsymbol{q}}$. Using the substitutions:

$$\boldsymbol{\Theta} = \begin{bmatrix}\boldsymbol{\theta}\\ \dot{\boldsymbol{\theta}}\end{bmatrix}; \qquad \boldsymbol{Q} = \begin{bmatrix}\boldsymbol{q}\\ \dot{\boldsymbol{q}}\end{bmatrix} \tag{24}$$

the state space representation can be put into a more concise form

$$\dot{\boldsymbol{\Theta}} = \boldsymbol{A}^*\boldsymbol{\Theta} + \boldsymbol{B}^*\boldsymbol{\tau}_{\mathrm{m}} + \boldsymbol{G}^*\boldsymbol{Q} \tag{25}$$

This resulting optimal control problem has $2N_J$ states, N_J constraint inputs, N_J constraints on the velocity state, and $8N_C$ constraints on the position state, and a quadratic cost function.

A. Cost

While the error term Γ_T is the same as in the rigid robot solution a new regularization term Γ_R is added on the system input $\boldsymbol{\tau}_m$, the input derivative $\dot{\boldsymbol{\tau}}_m$ and the motor velocities $\dot{\hat{\boldsymbol{\theta}}}$:

$$\Gamma_R = ||\boldsymbol{R}_{\tau_m}\boldsymbol{\tau}_m|| + ||\boldsymbol{R}_{\dot{\tau}_m}\dot{\boldsymbol{\tau}}_m|| + \left|\left|\boldsymbol{R}_{\dot{\theta}}\dot{\hat{\boldsymbol{\theta}}}\right|\right| \tag{26}$$

using regularization weights $\boldsymbol{R}_{\tau_m}$, $\boldsymbol{R}_{\dot{\tau}_m}$ and $\boldsymbol{R}_{\dot{\theta}}$. In order to handle singular configurations, a damped inverse of $\boldsymbol{J}_{C,i,l}$ is used. The regularization terms on $\dot{\hat{\boldsymbol{\theta}}}$ and $\hat{\boldsymbol{\tau}}_m$ stabilize the solution in the nullspace of this inverse.

The complete cost is given by the integral of the errors $\Gamma_T + \Gamma_R$ over the prediction horizon t_p:

$$\Gamma = \int_0^{t_p} \Gamma_T + \Gamma_R \tag{27}$$

Γ_T can be rewritten as a function of $\boldsymbol{\theta}$ and $\boldsymbol{q}$ using the following substitutions and dropping the time indices into

$$\Gamma_T = ||\boldsymbol{G}\left[\boldsymbol{P}\left[\boldsymbol{\Theta} - \boldsymbol{Q}\right] - \boldsymbol{W}_T\right]|| \,. \tag{28}$$

Then, we can extract the constant parts which depend on the disturbance and formulate the required quadratic form

$$\begin{aligned}
&\boldsymbol{\Theta}^T\boldsymbol{P}^T\boldsymbol{G}^T\boldsymbol{G}\boldsymbol{P}\boldsymbol{\Theta}-\\
&-2\left[\boldsymbol{Q}^T\boldsymbol{P}^T\boldsymbol{G}^T\boldsymbol{G}\boldsymbol{P}+\boldsymbol{W}_T\boldsymbol{G}^T\boldsymbol{G}\boldsymbol{P}\right]\boldsymbol{\Theta}+\\
&+\underbrace{\boldsymbol{Q}^T\boldsymbol{P}^T\boldsymbol{G}^T\boldsymbol{G}\boldsymbol{P}\boldsymbol{Q}+2\boldsymbol{W}_T\boldsymbol{G}^T\boldsymbol{G}\boldsymbol{P}\boldsymbol{Q}+\boldsymbol{W}_T^T\boldsymbol{G}^T\boldsymbol{G}\boldsymbol{W}_T}_{\text{const. w.r.t. }\boldsymbol{\Theta}}
\end{aligned} \tag{29}$$

which denotes the implemented cost function.

In the initial phase of the development of this controller, the authors tried to avoid the use of a model predictive approach. This was grounded on the idea that the desired torque and derivatives $\boldsymbol{\tau}_\mathrm{d}$, $\dot{\boldsymbol{\tau}}_\mathrm{d}$, and $\dot{\boldsymbol{\tau}}_\mathrm{d}$ required for the ESP* controller can be provided using the instantaneous force distribution and derivates of the associated input signals at least for the unconstrained case. Clearly this requires the minimization of relevant derivatives of the cost function (28). While this allows a dynamically consistent distribution of forces, there cannot be any guarantees w.r.t. the actuator constraints (7). To increase propagation of the derivatives across the model predictive controller in presence of course discretization of the horizon this idea is still useful. For this Γ_T is differentiated to penalize the mismatch of $\dot{\boldsymbol{W}}_T$ and $\dot{\boldsymbol{\Theta}}$

$$\Gamma_{T1} = \left|\left|\boldsymbol{G}_1\left[\dot{\boldsymbol{P}}\left[\boldsymbol{\Theta}-\boldsymbol{Q}\right]+\boldsymbol{P}\left[\dot{\boldsymbol{\Theta}}-\dot{\boldsymbol{Q}}\right]-\dot{\boldsymbol{W}}_T\right]\right|\right| \tag{30}$$

which depends on $\ddot{\boldsymbol{\theta}}$ for $\boldsymbol{D} > 0$ which then again depends on $\boldsymbol{\tau}_m$. $\dot{\boldsymbol{\Theta}}$ can be substituted with the system dynamics (23). This allows to split the cost function into a state and an input dependant part

$$\begin{aligned}
\Gamma_{T1} =&||\boldsymbol{G}_1[\dot{\boldsymbol{P}}\left[\boldsymbol{\Theta}-\boldsymbol{Q}\right]+\\
&+\boldsymbol{P}\left[\boldsymbol{A}^*\boldsymbol{\Theta}+\boldsymbol{B}^*\boldsymbol{\tau}_m+\boldsymbol{G}^*\boldsymbol{Q}-\dot{\boldsymbol{Q}}\right]-\dot{\boldsymbol{W}}_T]||
\end{aligned} \tag{31}$$

This can be repeated for $\ddot{\boldsymbol{W}}_T$. For series-elastic systems this shows a direct relation between $\ddot{\boldsymbol{W}}_T$ and the control input $\boldsymbol{\tau}_m$:

$$\begin{aligned}
\Gamma_{T2} =&||\boldsymbol{G}_2[\ddot{\boldsymbol{P}}\left[\boldsymbol{\Theta}-\boldsymbol{Q}\right]+2\dot{\boldsymbol{P}}\left[\dot{\boldsymbol{\Theta}}-\dot{\boldsymbol{Q}}\right]+\\
&+\boldsymbol{P}\left[\ddot{\boldsymbol{\Theta}}-\ddot{\boldsymbol{Q}}\right]-\ddot{\boldsymbol{W}}_T]||
\end{aligned} \tag{32}$$

where $\ddot{\boldsymbol{\Theta}}$ is

$$\begin{aligned}
\ddot{\boldsymbol{\Theta}} &= \boldsymbol{A}^*\dot{\boldsymbol{\Theta}} && +\boldsymbol{B}^*\dot{\boldsymbol{\tau}}_m+\boldsymbol{G}^*\dot{\boldsymbol{Q}}\\
&= \boldsymbol{A}^*\left[\boldsymbol{A}^*\boldsymbol{\Theta}+\boldsymbol{B}^*\boldsymbol{\tau}_m+\boldsymbol{G}^*\boldsymbol{Q}-\dot{\boldsymbol{Q}}\right] && +\boldsymbol{B}^*\dot{\boldsymbol{\tau}}_m+\boldsymbol{G}^*\dot{\boldsymbol{Q}}
\end{aligned} \tag{33}$$

Note that this cost function has the same redundancy properties as the cost function of the instantaneous force distribution.

B. Constraints

The constraints (3) on $\boldsymbol{W}_C$ which are already used in the balancer are applied for the prediction horizon. The constraints again depend on the desired contact state at this time of the prediction horizon. (21) is substituted into (3) to formulate the constraint as a function of $\boldsymbol{\theta}$.

Additional constraints on $\boldsymbol{\Theta}$ and $\boldsymbol{\tau}_m$ are added to the problem (7).

C. Extrapolation

The desired task forces $\boldsymbol{W}_T(t)$ and the link side state for the disturbance term in (23) and the contact states have to be provided for the horizon. We use the error dynamics of the system without contact force and actuator constraints for extrapolation. In essence, this means the force distribution problem is solved twice in the controller. First, the desired trajectory and associated contact forces are realized by an unconstrained system to obtain future link side states. Then the model predictive control approach uses this result and ensures feasibility w.r.t. the actuator and contact force constraints. The approach builds on the assumption that the prediction error in the unconstrained extrapolation is small.

If the desired contact set does not allow the generation of all task forces $\boldsymbol{W}_T$, the unconstrained extrapolation is no longer correct. This can however be resolved by defining stiffness and damping matrices of the task compliances such that only forces in feasible direction are generated [9].

The described predictive controller is now discretized and implemented as quadratic optimization problem with linear inequality constraints. The solution contains the inputs $\boldsymbol{\tau}_m$ from which using (23) and (5) the motor side states $\boldsymbol{\Theta}$ and the desired torques $\boldsymbol{\tau}_d$, $\dot{\boldsymbol{\tau}}_d$, and $\ddot{\boldsymbol{\tau}}_d$ are computed.

D. Horizon Length

To estimate how long the prediction horizon should be the actuator constraints and inputs are used. Let us consider the rather extreme example of a fully loaded joint spring being unloaded solely by motor displacement. This situation is described by the following simplified system dynamics with the scalar joint stiffness K and the scalar motor inertia B

$$B\ddot{\theta} = -K\theta + \tau_m \tag{34}$$

using $\theta(0) = {}^{\tau_\mathrm{max}}/_{K}$, $\dot{\theta}(0) = 0$ and $\tau_m = \tau_{\mathrm{m,max}}$. This is conservative as for any $D \neq 0$ (visco-elastic case) the required time is shorter. The system is limited to the maximum velocity (7) which typically creates an acceleration phase and a constant velocity phase. The required time $t_{\min}$ can be approximated with

$$t_{\min} = \frac{\tau_{\max}}{K\dot{\theta}} \tag{35}$$

In order to capture the actuator dynamics accurately, the MPC algorithm must have a prediction horizon with a length of $t_{\min}$ or longer. For an optimal solution for the case of a non-zero regularization term in the cost function, the time horizon has to be longer.

For the robot C-Runner with $\tau_{\mathrm{m,max}} = 400\mathrm{Nm}$, $\tau_{\max} = 200\mathrm{Nm}$, $\dot{\theta}_{\max} = 5.2^{\mathrm{rad}}/_{s}$, and $B = 1.62kg \cdot m^2$, we obtain a minimum length of $t_{\min} = 0.08s$.

VII. Results

The controller was implemented for the planar elastic bipedal robot C-Runner [16].

A. Implementation

For the dynamically consistent force distribution, the prediction horizon was discretized into 10 intervals with a constant interval of $0.01s$. This results in computation times below 1ms on recent desktop hardware which makes implementation of the approach on a real-time system feasible.

For extrapolation of the impedance forces the Cartesian mass Λ was assumed be constant. It was also assumed that $\boldsymbol{P}$ stays constant over the prediction horizon which is acceptable for low link-side velocities. As the time-constants of the foot impedances are very small due to small inertias, the extrapolation is unreliable and did not improve stability, hence they were neglected.

We use qpOASES [18] to implement the constraint optimization problem.

B. Simulation

A custom variable step multi-body simulation was used to verify the controller. For realistic simulation joint and motor side viscous and coulomb friction are implemented.

The conducted simulation task consist of shifting the load from a double stance with equal force distribution onto the left foot. Afterwards the right foot is lifted. Fig. 2 shows a comparison of the instantaneous force distribution (QP) and the dynamically consistent force distribution (MPC). The figure shows the transients of normal contact forces. When the static force distribution received the signal to disable the contact at $t = 0.9$s, it shifts all force onto the remaining leg. In contrast, the dynamically consistent approach received the set of active contacts over a preview window. This gives time to react in advance so that the contact force is already zero when the contact is disabled at $t = 0.97$s. The shape of the transient is defined by the cost function (28) and the constraints (7). The effect of the preview horizon discretization can be seen in Fig. 3 in the discontinuous system input $\boldsymbol{\tau}_m$. Fig. 3 also shows torque tracking performance of the structure preserving controller.

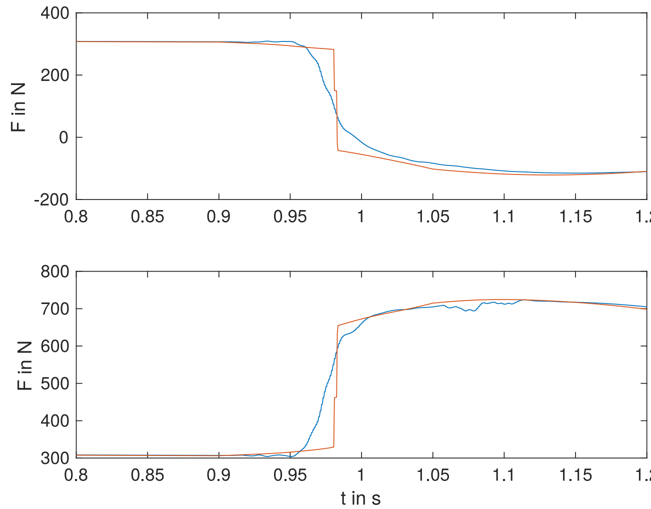

Fig. 2. Comparison of uninformed (rigid-body) force distribution (red) and dynamically consistent force distribution (blue). Top: left foot desired normal force. Bottom: right foot desired normal force.

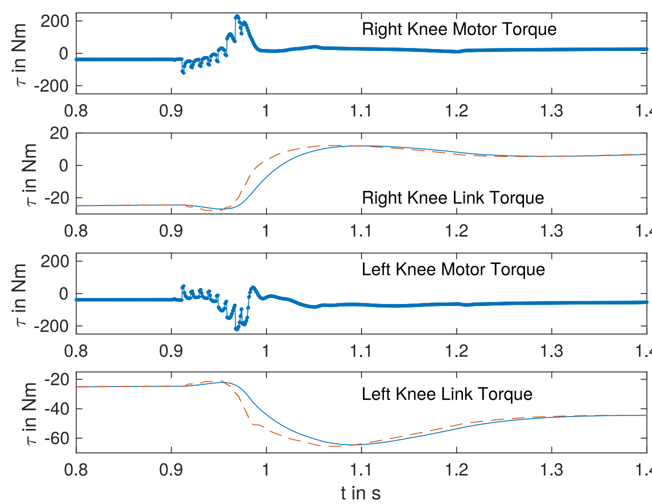

Fig. 3. Tracking of desired torque (dashed lines) with the structure preserving elastic joint controller. Top: Right Leg. Bottom: Left Leg.

VIII. Conclusion

This paper proposes a structure preserving balancing control scheme with dynamically consistent force distribution for series-elastic and visco-elastic humanoid robots. By applying MPC, the controller is able to meet the needs of considering the dynamics and constraints of the elastic actuators. This extends our previous work [9] in a way that contact transitions show a much more natural behavior.

References

[1] M. Mistry, J. Buchli, and S. Schaal, "Inverse dynamics control of floating base systems using orthogonal decomposition," in *IEEE Int. Conf. on Robotics and Automation*, May 2010, pp. 3406 – 3412.

[2] L. Righetti, J. Buchli, M. Mistry, M. Kalakrishnan, and S. Schaal, "Optimal distribution of contact forces with inverse dynamics control," *Int. J. of Robotics Research*, vol. 32, no. 3, pp. 280 – 298, 2013.

[3] L. Sentis, “Compliant control of whole-body multi-contact behaviors in humanoid robots,” in *Motion Planning for Humanoid Robots*, K. Harada, E. Yoshida, and K. Yokoi, Eds. Springer London, 2010, pp. 29–66.

[4] B. Henze, M. A. Roa, and C. Ott, “Passivity-based whole-body balancing for torque-controlled humanoid robots in multi-contact scenarios,” *The International Journal of Robotics Research*, vol. 35, no. 12, pp. 1522–1543, 2016.

[5] M. Keppler, D. Lakatos, C. Ott, and A. Albu-Schäffer, “A passivity-based approach for trajectory tracking and link-side damping of compliantly actuated robots,” in *Robotics and Automation (ICRA), 2016 IEEE International Conference on*. IEEE, 2016, pp. 1079–1086.

[6] ——, “A passivity-based controller for motion tracking and damping assignment for compliantly actuated robots,” in *Decision and Control (CDC), 2016 IEEE 55th Conference on*. IEEE, 2016, pp. 1521–1528.

[7] M. Laffranchi, N. Tsagarakis, and D. G. Caldwell, “A compact compliant actuator (compact) with variable physical damping,” in *Robotics and Automation (ICRA), 2011 IEEE International Conference on*. IEEE, 2011, pp. 4644–4650.

[8] M. Keppler, D. Lakatos, A. Werner, F. Loeffl, C. Ott, and A. Albu-Schäffer, “Visco-elastic structure preserving impedance (vespi) control for compliantly actuated robots,” in *European Control Conference (ECC), 2017*. IEEE, 2017.

[9] A. Werner, B. Henze, F. C. Loeffl, S. Leyendecker, and C. Ott, “Optimal and robust walking using intrinsic properties of a series-elastic robot,” in *IEEE-RAS International Conference on Humanoid Robots*, 2017.

[10] D. Kim, Y. Zhao, G. Thomas, and L. Sentis, “Assessing whole-body operational space control in a point-foot series elastic biped: Balance on split terrain and undirected walking,” *arXiv preprint arXiv:1501.02855*, 2015.

[11] D. Kim, Y. Zhao, G. Thomas, B. R. Fernandez, and L. Sentis, “Stabilizing series-elastic point-foot bipeds using whole-body operational space control,” *IEEE Transactions on Robotics*, vol. 32, no. 6, pp. 1362–1379, 2016.

[12] Y. Zhao and L. Sentis, “Passivity of time-delayed whole-body operational space control with series elastic actuation,” in *Humanoid Robots (Humanoids), 2016 IEEE-RAS 16th International Conference on*. IEEE, 2016, pp. 1290–1297.

[13] M. A. Hopkins, A. Leonessa, B. Y. Lattimer, and D. W. Hong, “Optimization-based whole-body control of a series elastic humanoid robot,” *International Journal of Humanoid Robotics*, vol. 13, no. 01, p. 1550034, 2016.

[14] B. G. Buss, K. A. Hamed, B. A. Griffin, and J. W. Grizzle, “Experimental results for 3d bipedal robot walking based on systematic optimization of virtual constraints,” in *American Control Conference (ACC), 2016*. IEEE, 2016, pp. 4785–4792.

[15] S. Rezazadeh, C. Hubicki, M. Jones, A. Peekema, J. Van Why, A. Abate, and J. Hurst, “Spring-mass walking with atrias in 3d: Robust gait control spanning zero to 4.3 kph on a heavily underactuated bipedal robot,” in *ASME 2015 dynamic systems and control conference*. American Society of Mechanical Engineers, 2015, pp. V001T04A003–V001T04A003.

[16] F. Loeffl, A. Werner, D. Lakatos, J. Reinecke, S. Wolf, R. Burger, T. Gumpert, F. Schmidt, C. Ott, M. Grebenstein, *et al.*, “The dlr c-runner: Concept, design and experiments,” in *2016 IEEE-RAS 16th International Conference on Humanoid Robots (Humanoids)*. IEEE, 2016, pp. 758–765.

[17] M. W. Spong, “Modeling and control of elastic joint robots,” *Journal of dynamic systems, measurement, and control*, vol. 109, no. 4, pp. 310–318, 1987.

[18] H. J. Ferreau, C. Kirches, A. Potschka, H. G. Bock, and M. Diehl, “qpoases: A parametric active-set algorithm for quadratic programming,” *Mathematical Programming Computation*, vol. 6, no. 4, pp. 327–363, 2014.

IX. Appendix

This appendix derives the closed loop dynamics of the structure preserving balancing controller for the case of a series-elastic robot. The system dynamics for link and motor side

$$\begin{bmatrix}\boldsymbol{M}_{\mathrm{b}} & \boldsymbol{M}_{\mathrm{b}q} & \boldsymbol{0}\\ \boldsymbol{M}_{\mathrm{b}q}^{\mathrm{T}} & \boldsymbol{M}_q & \boldsymbol{0}\\ \boldsymbol{0} & \boldsymbol{0} & \boldsymbol{B}\end{bmatrix}\begin{bmatrix}\ddot{\boldsymbol{b}}\\ \ddot{\boldsymbol{q}}\\ \ddot{\boldsymbol{\theta}}\end{bmatrix}+\begin{bmatrix}\boldsymbol{C}_b & \boldsymbol{C}_{bq} & \boldsymbol{0}\\ \boldsymbol{C}_{qb} & \boldsymbol{C}_q & \boldsymbol{0}\\ \boldsymbol{0} & \boldsymbol{0} & \boldsymbol{0}\end{bmatrix}\begin{bmatrix}\dot{\boldsymbol{b}}\\ \dot{\boldsymbol{q}}\\ \dot{\boldsymbol{\theta}}\end{bmatrix}+\begin{bmatrix}\boldsymbol{g_b}\\ \boldsymbol{g_q}\\ \boldsymbol{0}\end{bmatrix}+\begin{bmatrix}\boldsymbol{0} & \boldsymbol{0} & \boldsymbol{0}\\ \boldsymbol{0} & \boldsymbol{K} & -\boldsymbol{K}\\ \boldsymbol{0} & -\boldsymbol{K} & \boldsymbol{K}\end{bmatrix}\begin{bmatrix}\boldsymbol{b}\\ \boldsymbol{q}\\ \boldsymbol{\theta}\end{bmatrix}=\begin{bmatrix}\boldsymbol{0} & \boldsymbol{0} & \boldsymbol{0}\\ \boldsymbol{0} & \boldsymbol{0} & \boldsymbol{0}\\ \boldsymbol{0} & \boldsymbol{0} & \boldsymbol{0}\end{bmatrix}\begin{bmatrix}\dot{\boldsymbol{b}}\\ \dot{\boldsymbol{q}}\\ \dot{\boldsymbol{\theta}}\end{bmatrix}+\begin{bmatrix}\boldsymbol{0}\\ \boldsymbol{0}\\ \boldsymbol{\tau}_{\mathrm{m}}\end{bmatrix}+\begin{bmatrix}\boldsymbol{J}_{\mathrm{C},u}^{\mathrm{T}}\\ \boldsymbol{J}_{\mathrm{C},l}^{\mathrm{T}}\\ \boldsymbol{0}\end{bmatrix}\boldsymbol{W}_{\mathrm{C}} \tag{36}$$

with $\boldsymbol{b}$ the base coordinates, $\boldsymbol{q}$ the joint coordinates, $\boldsymbol{\theta}$ the motor coordinates, and the shorthands $\boldsymbol{J}_{C,u} = \left[\boldsymbol{J}_{C,1,u}^{\mathrm{T}}\ \boldsymbol{J}_{C,2,u}^{\mathrm{T}}\right]^{\mathrm{T}}$, $\boldsymbol{J}_{C,l} = \left[\boldsymbol{J}_{C,1,l}^{\mathrm{T}}\ \boldsymbol{J}_{C,2,l}^{\mathrm{T}}\right]^{\mathrm{T}}$, and $\boldsymbol{W}_C = \left[\boldsymbol{W}_{C,1}^{\mathrm{T}}\ \boldsymbol{W}_{C,2}^{\mathrm{T}}\right]^{\mathrm{T}}$. Substituting the ESP* coordinate transformation and the control law

$$\boldsymbol{\theta} = \boldsymbol{\eta} + \boldsymbol{K}^{-1}\boldsymbol{\tau}_d \qquad \boldsymbol{\tau}_m = \boldsymbol{B}\boldsymbol{K}^{-1}\ddot{\boldsymbol{\tau}}_d + \boldsymbol{\tau}_d - \boldsymbol{D}_\eta\dot{\boldsymbol{\eta}} \tag{37}$$

in (36) yields a system with the control input $\boldsymbol{\tau}_d$:

$$\begin{bmatrix}\boldsymbol{M}_{\mathrm{b}} & \boldsymbol{M}_{\mathrm{b}q} & \boldsymbol{0}\\ \boldsymbol{M}_{\mathrm{b}q}^{\mathrm{T}} & \boldsymbol{M}_q & \boldsymbol{0}\\ \boldsymbol{0} & \boldsymbol{0} & \boldsymbol{B}\end{bmatrix}\begin{bmatrix}\ddot{\boldsymbol{b}}\\ \ddot{\boldsymbol{q}}\\ \ddot{\boldsymbol{\eta}}\end{bmatrix}+\begin{bmatrix}\boldsymbol{C}_b & \boldsymbol{C}_{bq} & \boldsymbol{0}\\ \boldsymbol{C}_{qb} & \boldsymbol{C}_q & \boldsymbol{0}\\ \boldsymbol{0} & \boldsymbol{0} & \boldsymbol{0}\end{bmatrix}\begin{bmatrix}\dot{\boldsymbol{b}}\\ \dot{\boldsymbol{q}}\\ \dot{\boldsymbol{\eta}}\end{bmatrix}+\begin{bmatrix}\boldsymbol{g}_b\\ \boldsymbol{g_q}\\ \boldsymbol{0}\end{bmatrix}+\begin{bmatrix}\boldsymbol{0} & \boldsymbol{0} & \boldsymbol{0}\\ \boldsymbol{0} & \boldsymbol{K} & -\boldsymbol{K}\\ \boldsymbol{0} & -\boldsymbol{K} & \boldsymbol{K}\end{bmatrix}\begin{bmatrix}\boldsymbol{b}\\ \boldsymbol{q}\\ \boldsymbol{\eta}\end{bmatrix}=\begin{bmatrix}\boldsymbol{0} & \boldsymbol{0} & \boldsymbol{0}\\ \boldsymbol{0} & \boldsymbol{0} & \boldsymbol{0}\\ \boldsymbol{0} & \boldsymbol{0} & -\boldsymbol{D}_\eta\end{bmatrix}\begin{bmatrix}\dot{\boldsymbol{b}}\\ \dot{\boldsymbol{q}}\\ \dot{\boldsymbol{\eta}}\end{bmatrix}+\begin{bmatrix}\boldsymbol{0}\\ \boldsymbol{\tau}_{\mathrm{d}}\\ \boldsymbol{0}\end{bmatrix}+\begin{bmatrix}\boldsymbol{J}_{\mathrm{C},u}^{\mathrm{T}}\\ \boldsymbol{J}_{\mathrm{C},l}^{\mathrm{T}}\\ \boldsymbol{0}\end{bmatrix}\boldsymbol{W}_{\mathrm{C}} \tag{38}$$

as a preparation for the Cartesian control a coordinate transformation is applied which replaces the base coordinates $\boldsymbol{b}$ with the coordinates $\boldsymbol{x}$ which contain the CoM position and the base rotation and also replaces $\dot{\boldsymbol{q}}$ with Cartesian velocities $\dot{\boldsymbol{x}}_{\mathrm{T}}$ of the contact links, again including the rotation:

$$\begin{bmatrix}\dot{\boldsymbol{x}}\\ \dot{\boldsymbol{x}}_T\\ \dot{\boldsymbol{\eta}}\end{bmatrix}=\begin{bmatrix}\boldsymbol{L} & & \boldsymbol{0}\\ \boldsymbol{J}_{C,u} & \boldsymbol{J}_{C,l} & \boldsymbol{0}\\ \boldsymbol{0} & \boldsymbol{0} & \boldsymbol{I}\end{bmatrix}\begin{bmatrix}\dot{\boldsymbol{b}}\\ \dot{\boldsymbol{q}}\\ \dot{\boldsymbol{\eta}}\end{bmatrix} \tag{39}$$

with $\boldsymbol{L}$ the CoM Jacobian and mapping for the base rotation velocity, see [4] for details. Substituting this into (38) yields:

$$\begin{aligned}&\begin{bmatrix}\boldsymbol{\Lambda}_{\mathrm{x}} & \boldsymbol{\Lambda}_{\mathrm{x}T} & \boldsymbol{0}\\ \boldsymbol{\Lambda}_{\mathrm{x}T}^{\mathrm{T}} & \boldsymbol{\Lambda}_T & \boldsymbol{0}\\ \boldsymbol{0} & \boldsymbol{0} & \boldsymbol{B}\end{bmatrix}\begin{bmatrix}\ddot{\boldsymbol{x}}\\ \ddot{\boldsymbol{x}}_{\mathrm{T}}\\ \ddot{\boldsymbol{\eta}}\end{bmatrix}+\begin{bmatrix}\boldsymbol{C}_x & \boldsymbol{C}_{xT} & \boldsymbol{0}\\ \boldsymbol{C}_{Tx} & \boldsymbol{C}_T & \boldsymbol{0}\\ \boldsymbol{0} & \boldsymbol{0} & \boldsymbol{0}\end{bmatrix}\begin{bmatrix}\dot{\boldsymbol{x}}\\ \dot{\boldsymbol{x}}_{\mathrm{T}}\\ \dot{\boldsymbol{\eta}}\end{bmatrix}+\begin{bmatrix}m\boldsymbol{g}_0\\ \boldsymbol{0}\\ \boldsymbol{0}\end{bmatrix}+\\ &+\begin{bmatrix}\boldsymbol{0} & \boldsymbol{J}_{C,u}^{\mathrm{T}}\boldsymbol{J}_{C,l}^{-\mathrm{T}}\boldsymbol{K} & -\boldsymbol{J}_{C,u}^{\mathrm{T}}\boldsymbol{J}_{C,l}^{-T}\boldsymbol{K}\\ \boldsymbol{0} & \boldsymbol{J}_{C,l}^{-\mathrm{T}}\boldsymbol{K} & -\boldsymbol{J}_{C,l}^{-\mathrm{T}}\boldsymbol{K}\\ \boldsymbol{0} & -\boldsymbol{K} & \boldsymbol{K}\end{bmatrix}\begin{bmatrix}\boldsymbol{x}\\ \boldsymbol{g}(\boldsymbol{x},\boldsymbol{x}_{\mathrm{T}})\\ \boldsymbol{\eta}\end{bmatrix}+\begin{bmatrix}\boldsymbol{0} & \boldsymbol{0} & \boldsymbol{0}\\ \boldsymbol{0} & \boldsymbol{0} & \boldsymbol{0}\\ \boldsymbol{0} & \boldsymbol{0} & \boldsymbol{D}_\eta\end{bmatrix}\begin{bmatrix}\dot{\boldsymbol{x}}\\ \dot{\boldsymbol{x}}_{\mathrm{T}}\\ \dot{\boldsymbol{\eta}}\end{bmatrix}=\begin{bmatrix}\boldsymbol{0}\\ \boldsymbol{I}\\ \boldsymbol{0}\end{bmatrix}\boldsymbol{W}_{\mathrm{C}}+\begin{bmatrix}\boldsymbol{J}_{C,u}^{\mathrm{T}}\\ -\boldsymbol{I}\\ \boldsymbol{0}\end{bmatrix}(-\boldsymbol{J}_{C,l}^{-\mathrm{T}}\boldsymbol{\tau}_{\mathrm{d}})\end{aligned} \tag{40}$$

where $\boldsymbol{\Lambda}$ is the Cartesian mass matrix with parts corresponding to the CoM position and base rotation, denoted with x and parts corresponding to the task space of the contact links, denoted with T. Additionally $\boldsymbol{q} = \boldsymbol{g}(\boldsymbol{x}, \boldsymbol{x}_{\mathrm{T}})$ is the inverse kinematic mapping from task space into joint space. The balancing control law, given for simplicity for the regulation case

$$\begin{aligned}\boldsymbol{\tau}_d &= -\boldsymbol{J}_{C,l}^{\mathrm{T}}\boldsymbol{W}_d\\ m\boldsymbol{g}_0 &= \boldsymbol{J}_{C,u}^{\mathrm{T}}\boldsymbol{W}_d + \boldsymbol{K}_x(\boldsymbol{x}-\boldsymbol{x}_d) + \boldsymbol{D}_x(\dot{\boldsymbol{x}}-\dot{\boldsymbol{x}}_d)\end{aligned} \tag{41}$$

is substituted into (40) which yields:

$$\begin{aligned}&\boldsymbol{\Lambda}\begin{bmatrix}\ddot{\boldsymbol{x}}\\ \ddot{\boldsymbol{x}}_{\mathrm{T}}\\ \ddot{\boldsymbol{\eta}}\end{bmatrix}+\boldsymbol{C}\begin{bmatrix}\dot{\boldsymbol{x}}\\ \dot{\boldsymbol{x}}_{\mathrm{T}}\\ \dot{\boldsymbol{\eta}}\end{bmatrix}+\begin{bmatrix}\boldsymbol{0} & \boldsymbol{J}_{C,u}^{\mathrm{T}}\boldsymbol{J}_{C,l}^{-\mathrm{T}}\boldsymbol{K} & -\boldsymbol{J}_{C,u}^{\mathrm{T}}\boldsymbol{J}_{C,l}^{-T}\boldsymbol{K}\\ \boldsymbol{0} & \boldsymbol{J}_{C,l}^{-\mathrm{T}}\boldsymbol{K} & -\boldsymbol{J}_{C,l}^{-\mathrm{T}}\boldsymbol{K}\\ \boldsymbol{0} & -\boldsymbol{K} & \boldsymbol{K}\end{bmatrix}\begin{bmatrix}\boldsymbol{x}\\ \boldsymbol{g}(\boldsymbol{x},\boldsymbol{x}_{\mathrm{T}})\\ \boldsymbol{\eta}\end{bmatrix}+\\ &+\begin{bmatrix}\boldsymbol{K}_x & \boldsymbol{0} & \boldsymbol{0}\\ \boldsymbol{0} & \boldsymbol{0} & \boldsymbol{0}\\ \boldsymbol{0} & \boldsymbol{0} & \boldsymbol{0}\end{bmatrix}\begin{bmatrix}\boldsymbol{x}\\ \boldsymbol{x}_{\mathrm{T}}\\ \boldsymbol{\eta}\end{bmatrix}+\begin{bmatrix}\boldsymbol{D}_x & \boldsymbol{0} & \boldsymbol{0}\\ \boldsymbol{0} & \boldsymbol{0} & \boldsymbol{0}\\ \boldsymbol{0} & \boldsymbol{0} & \boldsymbol{D}_\eta\end{bmatrix}\begin{bmatrix}\dot{\boldsymbol{x}}\\ \dot{\boldsymbol{x}}_{\mathrm{T}}\\ \dot{\boldsymbol{\eta}}\end{bmatrix}=\begin{bmatrix}\boldsymbol{0}\\ \boldsymbol{I}\\ \boldsymbol{0}\end{bmatrix}\boldsymbol{W}_{\mathrm{C}}+\begin{bmatrix}\boldsymbol{0}\\ -\boldsymbol{W}_{\mathrm{d}}\\ \boldsymbol{0}\end{bmatrix}\end{aligned} \tag{42}$$

For the example situation with only one foot in contact the coordinate $\boldsymbol{x}_{\mathrm{T}}$ are now split into coordinates used for balancing ($\boldsymbol{x}_{\mathrm{T1}}$) and interaction ($\boldsymbol{x}_{\mathrm{T2}}$). Thus, the Cartesian impedance force only acts on the sub-rows associated with T2 and the desired forces on the contact links are

$$\boldsymbol{W}_{\mathrm{d}} = \begin{bmatrix}\boldsymbol{W}_{T1d}\\ \boldsymbol{K}_{T2}\boldsymbol{x}_{T2} + \boldsymbol{D}_{T2}\dot{\boldsymbol{x}}_{T2}\end{bmatrix} \tag{43}$$

with the still unknown contact force $\boldsymbol{W}_{T1d}$. Substituting (43) in (42) yields

$$\begin{aligned}&\boldsymbol{\Lambda}\begin{bmatrix}\ddot{\boldsymbol{x}}\\ \begin{bmatrix}\ddot{\boldsymbol{x}}_{\mathrm{T1}}\\ \ddot{\boldsymbol{x}}_{\mathrm{T2}}\end{bmatrix}\\ \ddot{\boldsymbol{\eta}}\end{bmatrix}+\boldsymbol{C}\begin{bmatrix}\dot{\boldsymbol{x}}\\ \begin{bmatrix}\dot{\boldsymbol{x}}_{\mathrm{T1}}\\ \dot{\boldsymbol{x}}_{\mathrm{T2}}\end{bmatrix}\\ \dot{\boldsymbol{\eta}}\end{bmatrix}+\begin{bmatrix}\boldsymbol{0} & \boldsymbol{J}_{C,u}^{\mathrm{T}}\boldsymbol{J}_{C,l}^{-\mathrm{T}}\boldsymbol{K} & -\boldsymbol{J}_{C,u}^{\mathrm{T}}\boldsymbol{J}_{C,l}^{-T}\boldsymbol{K}\\ \boldsymbol{0} & \boldsymbol{J}_{C,l}^{-\mathrm{T}}\boldsymbol{K} & -\boldsymbol{J}_{C,l}^{-\mathrm{T}}\boldsymbol{K}\\ \boldsymbol{0} & -\boldsymbol{K} & \boldsymbol{K}\end{bmatrix}\begin{bmatrix}\boldsymbol{x}\\ \boldsymbol{g}(\boldsymbol{x},\boldsymbol{x}_{\mathrm{T}})\\ \boldsymbol{\eta}\end{bmatrix}+\\ &+\begin{bmatrix}\boldsymbol{K}_x & \boldsymbol{0} & \boldsymbol{0}\\ \boldsymbol{0} & \begin{bmatrix}\boldsymbol{0} & \boldsymbol{0}\\ \boldsymbol{0} & \boldsymbol{K}_{\mathrm{T2}}\end{bmatrix} & \boldsymbol{0}\\ \boldsymbol{0} & \boldsymbol{0} & \boldsymbol{0}\end{bmatrix}\begin{bmatrix}\boldsymbol{x}\\ \begin{bmatrix}\boldsymbol{x}_{\mathrm{T1}}\\ \boldsymbol{x}_{\mathrm{T2}}\end{bmatrix}\\ \boldsymbol{\eta}\end{bmatrix}+\begin{bmatrix}\boldsymbol{D}_x & \boldsymbol{0} & \boldsymbol{0}\\ \boldsymbol{0} & \begin{bmatrix}\boldsymbol{0} & \boldsymbol{0}\\ \boldsymbol{0} & \boldsymbol{D}_{\mathrm{T2}}\end{bmatrix} & \boldsymbol{0}\\ \boldsymbol{0} & \boldsymbol{0} & \boldsymbol{D}_\eta\end{bmatrix}\begin{bmatrix}\dot{\boldsymbol{x}}\\ \begin{bmatrix}\dot{\boldsymbol{x}}_{\mathrm{T1}}\\ \dot{\boldsymbol{x}}_{\mathrm{T2}}\end{bmatrix}\\ \dot{\boldsymbol{\eta}}\end{bmatrix}=\begin{bmatrix}\boldsymbol{0}\\ \begin{bmatrix}\boldsymbol{W}_{\mathrm{T1}}-\boldsymbol{W}_{\mathrm{d1}}\\ \boldsymbol{W}_{\mathrm{T2}}\end{bmatrix}\\ \boldsymbol{0}\end{bmatrix}\end{aligned} \tag{44}$$

Finally the contact constraint is applied

$$\boldsymbol{0} = \begin{bmatrix}\boldsymbol{I} & \boldsymbol{0}\end{bmatrix}\begin{bmatrix}\dot{\boldsymbol{x}}_{\mathrm{T1}}\\ \dot{\boldsymbol{x}}_{\mathrm{T2}}\end{bmatrix} \tag{45}$$

which removes the sub-rows related to the coordinates in contact and the unknown contact force $\boldsymbol{W}_{T1d}$

$$\tilde{\boldsymbol{\Lambda}}\begin{bmatrix}\ddot{\boldsymbol{x}}\\ \ddot{\boldsymbol{x}}_{\mathrm{T2}}\\ \ddot{\boldsymbol{\eta}}\end{bmatrix}+\boldsymbol{C}\begin{bmatrix}\dot{\boldsymbol{x}}\\ \dot{\boldsymbol{x}}_{\mathrm{T2}}\\ \dot{\boldsymbol{\eta}}\end{bmatrix}+\begin{bmatrix}\boldsymbol{0} & \boldsymbol{J}_{C,u}^{\mathrm{T}}\boldsymbol{J}_{C,l}^{-\mathrm{T}}\boldsymbol{K} & -\boldsymbol{J}_{C,l}^{\mathrm{T}}\boldsymbol{J}_{C,l}^{-T}\boldsymbol{K}\\ \boldsymbol{0} & \boldsymbol{J}_{C,l}^{-\mathrm{T}}\boldsymbol{K} & -\boldsymbol{J}_{C,l}^{-\mathrm{T}}\boldsymbol{K}\\ \boldsymbol{0} & -\boldsymbol{K} & \boldsymbol{K}\end{bmatrix}\begin{bmatrix}\boldsymbol{x}\\ \boldsymbol{g}(\boldsymbol{x},\boldsymbol{x}_{\mathrm{T}})\\ \boldsymbol{\eta}\end{bmatrix}+\begin{bmatrix}\boldsymbol{K}_x & \boldsymbol{0} & \boldsymbol{0}\\ \boldsymbol{0} & \boldsymbol{K}_{\mathrm{T2}} & \boldsymbol{0}\\ \boldsymbol{0} & \boldsymbol{0} & \boldsymbol{0}\end{bmatrix}\begin{bmatrix}\boldsymbol{x}\\ \boldsymbol{x}_{\mathrm{T2}}\\ \boldsymbol{\eta}\end{bmatrix}+\begin{bmatrix}\boldsymbol{D}_x & \boldsymbol{0} & \boldsymbol{0}\\ \boldsymbol{0} & \boldsymbol{D}_{\mathrm{T2}} & \boldsymbol{0}\\ \boldsymbol{0} & \boldsymbol{0} & \boldsymbol{D}_\eta\end{bmatrix}\begin{bmatrix}\dot{\boldsymbol{x}}\\ \dot{\boldsymbol{x}}_{\mathrm{T2}}\\ \dot{\boldsymbol{\eta}}\end{bmatrix}=\begin{bmatrix}\boldsymbol{0}\\ \boldsymbol{W}_{\mathrm{T2}}\\ \boldsymbol{0}\end{bmatrix} \tag{46}$$